Rate Coefficient and Mechanism of the Gas Phase OH Hydrogen Abstraction Reaction from Formic Acid: A Quantum Mechanical Approach

ARTICLE *in* THE JOURNAL OF PHYSICAL CHEMISTRY A · OCTOBER 2002

Impact Factor: 2.69 · DOI: 10.1021/jp020297i

4 AUTHORS, INCLUDING:

Annia Galano
Metropolitan Autonomous University
152 PUBLICATIONS **3,287** CITATIONS

SEE PROFILE

Juan Raul Alvarez-Idaboy
Universidad Nacional Autónoma de México
121 PUBLICATIONS **2,138** CITATIONS

SEE PROFILE

Rate Coefficient and Mechanism of the Gas Phase OH Hydrogen Abstraction Reaction from Formic Acid: A Quantum Mechanical Approach

Annia Galano,[†,‡] J. Raúl Alvarez-Idaboy,*[,†] Ma. Esther Ruiz-Santoyo,[†] and Annik Vivier-Bunge[‡]

Instituto Mexicano del Petróleo, Eje Central Lázaro Cárdenas 152, 07730, México D. F., México, and Universidad Autónoma Metropolitana, Iztapalapa, 09340, México D. F., México

Received: January 30, 2002; In Final Form: July 11, 2002

Unrestricted second and fourth order Møller−Plesset perturbation theory (MP2 and MP4), density functional theory (B3LYP and BHandHLYP), coupled cluster (CCSD(T)), and quadratic configuration interaction (QCI) calculations have been performed using both the 6-311++G(d,p) and 6-311++G(2d,2p) basis sets, to study the OH hydrogen abstraction reaction from formic acid. A complex mechanism involving the formation of a very stable prereactive complex is proposed, and the rate coefficients are calculated over the temperature range 296−445 K, using classical transition state theory. The following expressions, in L mol^{-1} s^{-1}, are obtained for the acidic, for the formyl, and for the overall temperature-dependent rate constants: $k_I = (1.37 \pm 0.40) \times 10^7 \exp[(786 \pm 87)/T]$, $k_{II} = (5.93 \pm 1.39) \times 10^8 \exp[(-1036 \pm 72)/T]$, and $k = (5.28 \pm 2.35) \times 10^7 \exp[(404 \pm 125)/T]$, respectively. An extremely large tunneling factor results for the acidic path, as a consequence of the presence of a high and narrow effective activation barrier. The contribution of the formyl path to the overall rate coefficient, as well as the magnitude of the tunneling effect, explain the observed non-Arrhenius behavior.

Introduction

It has been reported that formic acid (HCOOH) is the most abundant carboxylic acid in the troposphere.[1] In wet deposition, along with acetic acid, it accounts for up to 18% of the total acidity in rain in some places.[2] Major sources of formic acid include direct emissions of biogenic byproducts and the photochemical oxidation of volatile organic compounds (VOCs). Some authors have reported that biogenic sources represent anywhere from 55 to almost 100% of the atmospheric formic acid,[3,4] depending on the urbanization of the area in question. Recently, it was demonstrated that under natural conditions the exchange of volatile acids between leaves and air is stimulated by light and, to a lesser degree, by temperature.[5,6] For example, greater quantities of formic acid are released in the morning than at nighttime. HCOOH is also formed by ozonolysis of several alkenes including ethene, propene, and isoprene.[7,8] Other suggested sources of formic acid are the photochemical processes that occur during long-range transport of anthropogenic hydrocarbons, in particular formaldehyde.[9]

The main chemical sink for atmospheric formic acid is the reaction with the hydroxyl radical. A complex reaction mechanism that includes two reaction channels has been suggested from experimental work:

$$HCOOH + {}^{\bullet}OH \rightarrow HCOO^{\bullet} + H_2O \qquad (I)$$

$$HCOOH + {}^{\bullet}OH \rightarrow {}^{\bullet}COOH + H_2O \qquad (II)$$

The kinetic studies of Wine et al.,[10] Jolly et al.,[11] and Singleton et al.[12] indicate that, at room temperature, the reaction pathway involving the abstraction of the acidic hydrogen (I) is dominant over the abstraction of the formyl hydrogen (II). The data from these studies are consistent and in good agreement with the room-temperature rate constant reported by Dagaut et al.[13] and are about 40−50% larger than the Zetzsch and Stuhl value.[14] However, all of them predict that, within experimental uncertainty, the temperature dependence of the rate coefficient is nearly zero.

Isotopic studies performed by Singleton et al.[12] showed that substitution of the acidic H by D has a very dramatic effect on the reactivity, whereas a similar substitution at the formyl group does not influence the reaction rate. These results suggest that the interaction between the OH radical and the acidic hydrogen is considerably stronger than the one between OH and the formyl hydrogen. However, the estimated rate constants for the direct abstraction of the formyl hydrogen of normal and deuterated formic acid are 2.4×10^7 and 0.41×10^7 L mol^{-1} s^{-1}, respectively, corresponding to about 9−11% of the observed total rate coefficients. Thus, the formyl hydrogen abstraction makes a small but significant contribution to the overall rate constant, and it should be taken into account.

Wine et al.[10] have suggested that the reaction mechanism is complex, based on their findings of a zero or slightly negative activation energy and a lack of isotope effect for the DCOOH + OH reaction. Jolly et al.[11] have discussed several reaction paths, including direct abstraction of the formyl and the acidic hydrogen. They also proposed a mechanism in which OH forms a hydrogen-bonded complex with formic acid, followed by transfer of the hydroxylic hydrogen within the adduct:

$$HCOOH + OH \leftrightarrow [HCOOH...OH] \rightarrow \text{products}$$

The strength of the hydrogen bond interactions between OH and the target molecule is responsible for the magnitude of the prereactive complex stabilization. In the case of the HCOOH + OH reaction, a large stabilization of the prereactive complex

* To whom correspondence should be addressed. E-mail: jidaboy@imp.mx.
† Instituto Mexicano del Petróleo.
‡ Universidad Autónoma Metropolitana.

10.1021/jp020297i CCC: $22.00
Published on Web 09/25/2002

is expected to occur. The importance of these complexes in several radical−molecule bimolecular reactions has been described, for example in the case of the reactions of the OH radical with alkenes,[15] toluene,[16] aldehydes,[17] and, more recently, amino acids.[18] The existence of the prereactive complex may be at the origin of a large tunneling effect.[17] Indeed, the adiabatic energy barrier for a bimolecular hydrogen (deuterium) transfer process, if such a complex were not formed, would be lower, and consequently, the tunneling effect would also be smaller.

Singleton et al.[12] found a zero Arrhenius activation energy for the HCOOH + OH reaction and a small positive value for DCOOD + OD. The difference in the temperature dependence of the rate coefficients between the normal and deuterated formic acid with OH could be explained if a more important tunneling effect were found for reaction path (I) than for the abstraction from the formyl group (reaction II). The curvature of the Arrhenius plot is generally an indication that tunneling must be taken into account.

It is also interesting to point out that experimental results indicate that the rate coefficient of the HCOOH + OH reaction is approximately 10 times smaller than the one for the HCHO + OH reaction.[19,20] Because the measured activation energy of HCHO + OH is about zero, one would expect a larger and positive Ea value for HCOOH + OH, in disagreement with the experimental values.[10,12]

The need for a quantum mechanical study of the mechanism of the HCOOH + OH has been pointed out in experimental works.[11,12] Electronic molecular calculations of the potential energy surface along the different reaction channels may be performed. They could explain why the abstraction of the hydrogen atom from the acidic group is predominant over abstraction from the formyl group, although the C−H bond strength is weaker than the O−H bond strength by about 14 kcal/mol. They might also explain why the activation energy of the HCHO + OH is larger than the one for HCOOH + OH.

In this work, the gas-phase reaction mechanism of the OH hydrogen abstraction from formic acid is studied using accurate quantum chemistry methods. Energy profiles are calculated along two possible paths corresponding to reactions I and II. The Arrhenius parameters, tunneling corrections, and rate constants are obtained and compared with the experimental data. The efficiency of different approximation levels of theory is also tested.

Methodology

Electronic structure calculations have been performed with the Gaussian 98[21] program using the B3LYP and BHandHLYP hybrid HF-density functionals, as well as the ab initio MP2, MP4(SDQ), and QCISD methods with the 6-311++G(d,p) and 6-311++G(2d,2p) basis sets. Restricted calculations were used for closed shell systems, and unrestricted ones were used for open shell systems. All stationary points were fully optimized using the methods cited above and the 6-311++G(d,p) basis set, except with the MP2 method, in which case the larger 6-311++G(2d,2p) basis set was used. Single-point CCSD(T) energy calculations were also performed at the 6-311++G(2d,2p) level of theory, at several optimized geometries.

Frequency calculations were carried out for all of the stationary points at the DFT and MP2(FC) levels of theory. Local minima and transition states were identified by the number of imaginary frequencies (NIMAG = 0 or 1, respectively). Zero-point energies (ZPE) and thermal corrections to the energy (TCE) at 298.15K were included in the determination of activation energies and heats of reaction, respectively.

TABLE 1: Relevant Coordinates of the Reactant Complexes (RC) Optimized with Different Methods and the 6-311++G(d,p) Basis Set[a]

coordinate	B3LYP	BH&HLYP	MP2	MP4	QCISD
		$RC_{(I)}$			
r(HCOO**H**−**O**H**)**	1.76	1.98	1.94	2.06	2.02
r(H_2CO**O**−**H**O**)**	2.37	2.01	2.00	2.48	2.43
		$RC_{(II)}$			
r(H_2CO**O**−**H**O**)**	2.04	1.99	2.07	2.10	2.10

[a] For the MP2 method, the 6-311++G(2d,2p) was used.

Because unsatisfactory results were obtained with the B3LYP and MPn methods for the HCOO radical, calculations were also performed using the Gaussian-3 (G3) theory.[22] The latter is the third in a series of Gx methods for the calculation of molecular energies. It is a composite technique in which a sequence of well-defined ab initio molecular orbital calculations is performed, to arrive at the total energy of a given molecular species. In this method, geometries are determined using second-order Møller−Plesset perturbation theory. Correlation level calculations are done using Møller−Plesset perturbation theory up to fourth-order and quadratic configuration interaction. Large basis sets, including multiple sets of polarization functions, are used in the correlation calculations.

The heats of reaction were also calculated using the ROMP2 method, because unstable wave functions were obtained with all of the spin unrestricted methods.

The rate coefficients were calculated using conventional transition state theory (CTST) implemented in the Rate 1.1 program.[23] The vibrational partition functions were corrected by replacing some of the large amplitude vibrations by the corresponding hindered internal rotations. Because the HCOOH + OH reaction has a relatively high barrier and it is studied at room temperature, the above methodology should be adequate to describe it. In this work, tunneling corrections were calculated with an asymmetric Eckart function barrier. It is assumed that neither mixing nor crossover between different pathways occurs. Thus, the overall rate constant (k), which measures the rate of OH disappearance, can be determined by summing the rate coefficients calculated for the two pathways.[24]

The temperature dependence of k was also studied, and Arrhenius parameters were determined.

Results and Discussion

Geometries. The geometries of reactants, reactant complexes, transition states, and products were fully optimized using all the tested methods. Except for transition states, the stationary point geometries do not show a strong dependence on the optimization method (Table 1). All of them are shown in Figure 1, optimized at MP4/6-311++G(d,p). It can be observed that the acidic reactant complex ($RC_{(I)}$) is stabilized by two hydrogen bonds: one between the H atom of the COOH group and the O of the OH radical and the other between the carboxylic oxygen of the acidic group and the H of the OH radical. The first one is slightly stronger than the second one (Figure 1). In the formyl reactant complex ($RC_{(II)}$), only one hydrogen bond interaction occurs, between the H of the OH radical and one of the oxygen atoms of the acidic group.

With all of the tested methods, hydrogen bond-like interactions that stabilize the transition state structures were found (Figure 1). This interaction is stronger for $TS_{(I)}$ than for $TS_{(II)}$, because the H···O distance in the former is about 1 Å shorter than in the latter. In all cases, the structure of the formyl transition state ($TS_{(II)}$) was found to be planar. The acidic

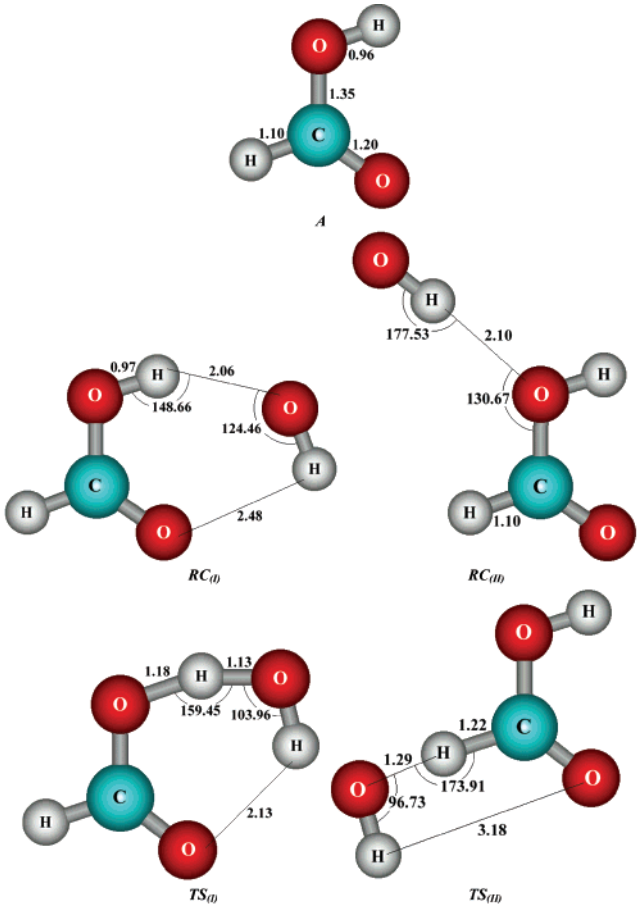

Figure 1. Geometries of the stationary points of the OH hydrogen abstraction reaction from formic acid, optimized at the MP4/6-311++G(d,p) level.

TABLE 2: Relevant Coordinates of the Transition Structures, *L* Parameters, and Imaginary Frequencies (cm^{-1})[a]

coordinate	B3LYP	BH&HLYP	MP2	MP4	QCISD
		$TS_{(I)}$			
r(OH)	1.19	1.22	1.17	1.18	1.21
r(HO)	1.23	1.17	1.13	1.13	1.12
a(OHO)	155.45	154.30	155.38	159.45	158.92
d(OHOH)	86.52	88.04	0.00	0.00	0.00
L(O)	0.81	1.20	1.17	1.24	1.55
ν_i	−1357.7	−1983.6	−3171.8		
		$TS_{(II)}$			
r(CH)	1.16	1.24	1.20	1.22	1.22
r(HO)	1.48	1.26	1.31	1.29	1.30
a(CHO)	177.14	175.26	170.73	173.91	175.42
d(CHOH)	0.00	0.00	0.00	0.16	0.02
L(C)	0.12	0.48	0.32	0.37	0.35
ν_i	−174.4	−1896.2	−2319.3		

[a] Both the geometry optimizations and frequency calculations were performed with the different methods using the 6-311++G(d,p) basis set. For the MP2 method, the 6-311++G(2d,2p) basis set was used.

transition state ($TS_{(I)}$) is described as planar by the MP2, MP4, and QCISD optimization methods but not by the DFT ones. Both hybrid density functional methods predict a dihedral angle OHOH of about 90° (Table 2). The possible planar structure was also modeled within the DFT formalism, and it was found that these methods describe it as a second-order saddle point; that is, two imaginary frequencies are found. In the same way, the nonplanar $TS_{(I)}$ structure is described as a second-order saddle point by the MPn methods tested in this work. This contradiction suggests that one of the structures is an artifact of the calculation. According to the results reported here, it seems that the DFT methods do not describe this transition state structure correctly.

Following refs 25 and 26, the *L* parameters for acidic and formyl hydrogen abstractions are defined as

$$L(\mathrm{O}) = \frac{\delta r(\mathrm{OH})}{\delta r(\mathrm{HO})} \quad (1)$$

and

$$L(\mathrm{C}) = \frac{\delta r(\mathrm{CH})}{\delta r(\mathrm{HO})} \quad (2)$$

In these equations, δr(OH) and δr(CH) represent variations, along both channels, in the bond distance between transition states and reactants for the bond that is breaking, whereas δr(HO) is the variation in the bond distance between transition states and products for the bond that is being formed. A value of *L* greater than 1 indicates that the transition state structure is product-like. All of the tested methods, with the exception of B3LYP (Table 2), predict $L(\mathrm{O}) > 1$ and $L(\mathrm{C}) < 1$. In general, the better the optimization method, the larger *L* is, and this trend is more significant for the HCOO−H abstraction than for the H−COOH. Consequently, the acidic abstraction should be endothermic and the formyl one exothermic, according to these results and to the Hammond Postulate.

Energies. Total electronic energies, zero point vibration corrections (ZPE), and thermal corrections to the energy (TCE) at 298.15 K of all of the stationary points are given in Table 3 parts a and b, for all of the methods employed in this work.

Relative energies, in kcal/mol, of the acidic and formyl channels of the HCOOH + OH reaction are shown in Table 4. The high stabilization energies for both abstraction paths (E_{-1} and E_{-3}) show, unambiguously, that the mechanism of this reaction is complex. The reaction path takes place in two steps, the first one leading to the formation of the prereactive complex (or reactants complex, RC) and the second one yielding the corresponding radical and water. The equations representing the two different channels are the following:

Acidic Abstraction

$$\text{Step A: } \mathrm{HCOOH + OH^{\bullet}} \underset{k_{-1}}{\overset{k_1}{\rightleftharpoons}} \mathrm{[HCOOH\cdots OH^{\bullet}]} \quad \text{(Ia)}$$

$$\text{Step B: } \mathrm{[HCOOH\cdots OH^{\bullet}]} \xrightarrow{k_2} \mathrm{HCOO^{\bullet} + H_2O} \quad \text{(Ib)}$$

Formyl Abstraction

$$\text{Step A: } \mathrm{HCOOH + OH^{\bullet}} \underset{k_{-3}}{\overset{k_3}{\rightleftharpoons}} \mathrm{[OH^{\bullet}\cdots HCOOH]} \quad \text{(IIa)}$$

$$\text{Step B: } \mathrm{[OH^{\bullet}\cdots HCOOH]} \xrightarrow{k_4} \mathrm{H_2O + {}^{\bullet}COOH} \quad \text{(IIb)}$$

In Table 4, the stabilization energy of the prereactive complex for channel I (acidic hydrogen abstraction) is seen to be higher than for channel II (formyl abstraction), as expected from the interactions described in the previous section. Most of the methods predict an acidic stabilization of about 4.8 kcal/mol and a formyl stabilization of about 1.8 kcal/mol, suggesting that, in the $RC_{(I)}$, the two hydrogen bond interactions are not additive but rather synergetic. The largest stabilization is predicted at the PMP2 level, being the energy gap between $RC_{(I)}$ and the isolated reactants of 6.14 kcal/mol. The magnitude of any of these stabilizations is large enough to cause a significant

TABLE 3: Total Energies (*E*), Zero-Point Energy Correction (ZPE), and Thermal Correction to the Energy (TCE) at 298.15 K, in Hartrees, for the Two Channels in the Hydrogen Abstraction Reaction from Formic Acid by OH Radicals

		HCOOH	OH	$RC_{(I)}$	$RC_{(II)}$	$TS_{(I)}$	$TS_{(II)}$
a. Total Energies (*E*)							
CCSD(T)/6-311++G(2d,2p) //B3LYP/6-311++G(d,p)		−189.4339474	−75.6148928	−265.0579950	−265.0538019	−265.0416431	−265.0417534
CCSD(T)/6-311++G(2d,2p) //BH&HLYP/6-311++G(d,p)		−189.4329023	−75.6148704	−265.0587562	−265.0534065	−265.0410952	−265.0397777
PMP2/6-311++G(2d,2p) //MP2/6-311++G(2d,2p)		−189.4064063	−75.5991671	−265.0187309	−265.0105340	−264.9923932	−264.9937925
PMP4/6-311++G(2d,2p) //MP4/6-311++G(d,p)		−189.4396847	−75.6152020	−265.0636900	−265.0599140	−265.0424500	−265.0445460
CCSD(T)/6-311++G(2d,2p) //MP2/6-311++G(2d,2p)		−189.4340631	−75.6149061	−265.0583297	−265.0539747	−265.0358597	−265.0401453
CCSD(T)/6-311++G(2d,2p) //MP4/6-311++G(d,p)		−189.4340326	−75.6149176	−265.0581391	−265.0539468	−265.0356069	−265.0404624
CCSD(T)/6-311++G(2d,2p) //QCISD/6-311++G(d,p)		−189.4340278	−75.6149175	−265.0582813	−265.0539480	−265.0356971	−265.0403600
b. Zero Point Energy Correction (ZPE) and Thermal Correction to the Energy (TCE) at 298.15 K							
B3LYP/6-311++G(D,p)	ZPE	0.033705	0.008457	0.045448	0.043940	0.041931	0.041497
	TCE	0.036876	0.010818	0.050784	0.049358	0.046338	0.046916
BH&HLYP/6-311++G(d,p)	ZPE	0.035257	0.008844	0.047332	0.046345	0.044235	0.040820
	TCE	0.038393	0.011204	0.052689	0.052440	0.048417	0.046209
MP2/6-311++G(2d,2p)	ZPE	0.033978	0.008702	0.046048	0.044750	0.040515	0.039724
	TCE	0.037150	0.011062	0.051392	0.050959	0.045041	0.045119

TABLE 4: Relevant Barriers, Including the ZPE (kcal/mol)

	E_{-1}	E_2	$E^{eff}_{a(I)}$	E_{-3}	E_4	$E^{eff}_{a(II)}$
CCSD(T)/6-311++G(2d,2p) //B3LYP/6-311++G(d,p)	3.68	8.05	4.37	2.00	6.03	4.03
CCSD(T)/6-311++G(2d,2p) //BH&HLYP/6-311++G(d,p)	4.86	9.14	4.27	2.13	5.08	2.96
PMP2/6-311++G(2d,2p) //MP2/6-311++G(2d,2p)	6.14	13.06	6.91	1.81	7.35	5.54
PMP4/6-311++G(2d,2p) //MP4/6-311++G(d,p)	4.50	10.94	6.44	1.84	6.49	4.63
CCSD(T)/6-311++G(2d,2p) //MP2/6-311++G(2d,2p)	4.85	11.72	6.87	1.84	5.52	3.68
CCSD(T)/6-311++G(2d,2p) //MP4/6-311++G(d,p)	4.74	11.76	7.01	1.84	5.31	3.47
CCSD(T)/6-311++G(2d,2p) //QCISD/6-311++G(d,p)	4.83	11.79	6.96	1.84	5.37	3.53

TABLE 5: Heats of Reaction, Including the TCE Corrections (kcal/mol) at 298.15 K

	ΔH_I	ΔH_{II}
CCSD(T)/6-311++G(2d,2p) //B3LYP/6-311++G(d,p)	−4.80	−17.29
CCSD(T)/6-311++G(2d,2p) //BH&HLYP/6-311++G(d,p)	−3.16	−18.88
PMP2/6-311++G(2d,2p) //MP2/6-311++G(2d,2p)	−10.85	−23.52
PMP4/6-311++G(2d,2p) //MP4/6-311++G(d,p)	−7.48	−20.13
CCSD(T)/6-311++G(2d,2p) //MP2/6-311++G(2d,2p)	−4.25	−18.84
CCSD(T)/6-311++G(2d,2p) //MP4/6-311++G(d,p)	−2.81	−18.82
CCSD(T)/6-311++G(2d,2p) //QCISD/6-311++G(d,p)	−2.09	−17.41
G3	−6.43	−19.36
ROMP2	−14.87	−23.81

increase of the tunneling effect, with respect to the one we would expect if the prereactive complexes were not taken into account. All of the methods predict that the effective activation energy of the acidic path ($E^{eff}_{a(I)}$) is higher than the corresponding one for the formyl path ($E^{eff}_{a(II)}$).

In general, the difference between the calculated values, along the two paths, increases as the level of theory improves. The calculated values of $E^{eff}_{a(I)}$ vary from 4.3 to 7.0, whereas those for $E^{eff}_{a(II)}$ go from 2.96 to 4.63 kcal/mol. They are in agreement with the O−H and C−H bond strengths but differ considerably from the experimental Arrhenius activation energies, $E^{Exp}_{a(I)} = 0.2$ kcal/m and $E^{Exp}_{a(II)} = 1.2$ kcal/mol, reported in ref 12. Moreover, the calculated values are in contradiction with a bond energy-bond order calculation by Jolly et al.,[11] predicting $E^{Exp}_{a(I)} < E^{Exp}_{a(II)}$ by about 1−2 kcal/mol. It is also in contradiction with the isotopic study by Singleton et al.,[12] which proved unambiguously that substitution of the acidic H by D had a much more important effect on the rate of the reaction than substitution at the formyl hydrogen.

The cause of these apparent contradictions is, in our opinion, 3-fold:

(i) The mechanism of the OH + HCOOH reaction is complex, with a first step leading to the formation of a very stable prereactive complex in equilibrium with the reactants, followed by a second step corresponding to the hydrogen abstraction.

(ii) The two different channels may occur simultaneously.

(iii) The effective height of the energy barriers is considerably larger than the one obtained in the direct bimolecular reaction, because both prereactive complexes are very stable. Thus, significant tunneling effects can be expected to occur.

The calculation of the rate coefficients of the hydrogen abstraction paths and the determination of their respective weight in the overall reaction, as well as a temperature dependence study, could explain the experimental results.

Concerning the heats of the reactions (Table 5), all of the methods predict both reaction paths to be exothermic. The calculated G3 heats of reaction are found to be $\Delta H_{(I)} = -6.72$ and $\Delta H_{(II)} = -17.52$ kcal/mol. The difference between the theoretical heats of reaction of the two channels is in good agreement with the experimental relative strength of the C−H and O−H bonds: the bond dissociation energy of O−H is about 14 kcal/mol larger than the C−H one (92.6 and 106.6 kcal/mol, respectively).[27] The experimental heats of reaction obtained from the corresponding heats of formation are $\Delta H_{(I)} = -12.7$ and $\Delta H_{(II)} = -27.7$ kcal/mol.[27] Recent data[28] for the formyl channel lead to $\Delta H_{(II)} = -28.02$ kcal/mol. No direct experimental data are available for the heat of formation of HC(O)O, but Benson has given an estimate of its magnitude.[27] An

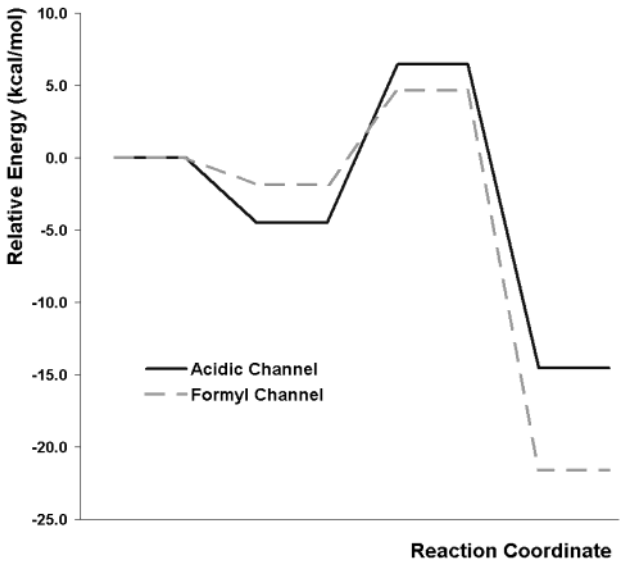

Figure 2. Reaction profiles of the acidic and formyl abstraction, at the PMP4/6-311++G(2d,2p)//MP4/6-311+G(d,P) level.

alternative way to estimate the heat of formation of HC(O)O is to assume that the O−H bond dissociation energy of formic acid is the same as the one for acetic acid.[29] The IUPAC thermochemistry section[28] reports heats of formation of acetic acid and $CH_3C(O)O$ radical, which result in an O−H bond dissociation energy of 105.8 (±1) kcal mol^{-1}. The use of this O−H bond dissociation energy for the formic acid system leads to $\Delta H_{(I)} = -13.0$ kcal/mol.

The calculated heats of reaction are not in good agreement with the values obtained from the experimental heats of formation, with the exception of those calculated at the PMP2/6-311++G(2d,2p)//MP2/6-311++G(2d,2p) level, which are $\Delta H_{(I)} = -10.85$ kcal/mol and $\Delta H_{(II)} = -23.52$ kcal/mol. Apparently, the problem has to do with the inability of the unrestricted methods to properly describe the C_{2v} structure of one of the products: the formyloxyl (HCOO) radical. Difficulties were encountered when trying to optimize its geometrical parameters. It was observed that unrestricted methods applied to the HCOO radical yield wave functions that are unstable, and the calculations do not converge to the correct product. Such a behavior, known as symmetry breaking or doublet instability, has been observed in other highly symmetric radical structures, and it has been extensively studied for the formyloxyl radical.[30−40] In an effort to improve our results, a restricted open MP2 calculation ROMP2/6-311++G(2d,2p) was performed, and the ROMP2 energy for the HCOO radical turned out to be appreciably lower than the one obtained with UMP2. Taking the corresponding geometry as a starting point, new UMP2 calculations were performed, but the wave function was found to be unstable. For that reason, in the calculation of the tunneling effect described below, we used the ROMP2 energy gap between RC_{II} and the corresponding products.

We noticed above that the transition state for acidic abstraction is product-like**,** and according to the Hammond postulate, we should expect $\Delta H_{(I)} > 0$. The Hammond postulate works best when the force constant matrixes associated with the reactants and products in an elementary process are not very different,[41−44] which is not the case. In addition, although it applies to most chemical reactions, some failures have been reported.[45−48]

Reaction profiles for both channels are shown in Figure 2. They show that the overall activation energy for the formyl abstraction is considerably lower than the one for the acidic abstraction. In addition, the energy release is larger for channel II. According to these features, the formyl channel should be predominant, in contradiction with the experimental results. Only a large difference in the tunneling effects across the two barriers could explain the observed experimental results. Indeed, because the barrier along the acidic reaction path is higher and narrower (as suggested by a much larger imaginary frequency, Table 2), the tunneling factor is expected to be considerably larger for path I than for path II. This could lead to the acidic rate coefficient being larger than the formyl one.

Kinetics. According to the complex mechanism proposed above, both channels involve a fast preequilibrium between reactants (R) and the prereactive complexes (RC_I and RC_{II}), followed by the elimination of a water molecule. A steady-state analysis applied to the prereactive complexes leads to the following rate coefficient for the overall reaction (k):

$$k = k_I + k_{II} = \frac{k_1 k_2}{k_{-1}} + \frac{k_3 k_4}{k_{-3}} \quad (3)$$

The combined rate coefficient could present a non-Arrhenius behavior. Nevertheless each reaction path could still be Arrhenius-type.

Because E_1 and E_3 are equal to zero, the net activation energy of each abstraction path (Ea_I and Ea_{II}) is

$$Ea_I = E_2 - E_{-1} = (E_{TS_I} - E_{RC_I}) - (E_R - E_{RC_I}) = E_{TS_I} - E_{R_I} \quad (4)$$

$$Ea_{II} = E_4 - E_{-3} = (E_{TS_{II}} - E_{RC_{II}}) - (E_R - E_{RC_{II}}) = E_{TS_{II}} - E_{R_{II}} \quad (5)$$

where E_R, E_{RC_I}, $E_{RC_{II}}$, E_{TS_I}, and $E_{TS_{II}}$ are the total energies of the reactants, prereactive complexes, and transition states, respectively.

The rate coefficients for the acidic and formyl abstraction may be expressed as

$$k_I = K_{eqI} \cdot k_2 = \kappa_2 \frac{k_B T}{h} \frac{Q_{TS_I}}{Q_R} e^{-(E_{TSI} - E_R)/RT} = \kappa_2 A e^{-Ea_I/RT} \quad (6)$$

$$k_{II} = K_{eqII} \cdot k_2 = \kappa_4 \frac{k_B T}{h} \frac{Q_{TS_{II}}}{Q_R} e^{-(E_{TSII} - E_R)/RT} = \kappa_4 A e^{-Ea_{II}/RT} \quad (7)$$

where K_{eq} are the equilibrium constants, Q is the partition functions, κ_2 and κ_4 are the tunneling factors, and k_B and h are the Boltzmann and Planck constants, respectively.

The tunneling effects, the rate coefficients, and the formyl branching ratio for the OH hydrogen abstraction reaction from formic acid are reported in Table 6, as obtained with all of the methods used in this work. The activation energies include the ZPE correction. The ratios Q_{TS_I}/Q_R and $Q_{TS_{II}}/Q_R$ of the Gaussian output have been corrected to take into account internal rotations.

The tunneling factor depends on the abstraction site and on the method of calculation. When κ is calculated from DFT results its value is much lower than when it is calculated from MP2 results (Table 6). This difference is mainly due to the fact that DFT predicts imaginary frequencies at the transition states that are appreciably lower than the ones obtained with the MP2 formalism. With the exception of DFT methods, the acidic tunneling corrections are huge, κ_2 is of the order of 10^3, whereas for the formyl path, κ_4 is also quite large compared to standard

TABLE 6: Tunneling Factors, Rate Coefficients, and Formyl Branching Ratio (Γ_{II}) at 298.15 K, and Arrhenius Parameters over the Temperature Range 296−445 K

	κ_2	κ_4	$k_{(I)}$ (L mol^{-1} s^{-1})	$k_{(II)}$ (L mol^{-1} s^{-1})	$k = k_{(I)} + k_{(II)}$ (L mol^{-1} s^{-1})	Ea^{Arr}	A	Γ_{II}
CCSD(T)/6-311++G(2d,2p) //B3LYP/6-311++G(d,p)	8.3	1.0	3.36×10^6	2.91×10^5	3.65×10^6	2.77	7.31×10^9	0.08
CCSD(T)/6-311++G(2d,2p) //BH&HLYP/6-311++G(d,p)	91.5	18.8	4.08×10^7	2.85×10^7	6.93×10^7	1.22	2.00×10^9	0.41
PMP2/6-311++G(2d,2p) //MP2/6-311++G(2d,2p)	14251.8	52.7	1.98×10^8	1.91×10^7	2.17×10^8	−0.80	5.28×10^7	0.08
PMP4/6-311++G(2d,2p) //MP4/6-311++G(d,p)	4647.9	35.9	1.42×10^8	5.98×10^7	2.02×10^8	0.36	3.58×10^8	0.30
CCSD(T)/6-311++G(2d,2p) //MP2/6-311++G(2d,2p)	8063.6	13.9	1.20×10^8	1.16×10^8	2.36×10^8	0.08	8.26×10^8	0.49
CCSD(T)/6-311++G(2d,2p) //MP4/6-311++G(d,p)	8108.5	20.5	9.46×10^7	2.43×10^8	3.38×10^8	0.74	1.15×10^9	0.72
CCSD(T)/6-311++G(2d,2p) //QCISD/6-311++G(d,p)	8281.7	21.2	1.07×10^8	2.27×10^8	3.34×10^8	0.69	1.04×10^9	0.68
exp					$(2.78 \pm 0.47) \times 10^8$ [a] $(2.97 \pm 0.17) \times 10^8$ [b] $(2.69 \pm 0.17) \times 10^8$ [c] $(2.23 \pm 0.24) \times 10^8$ [d] $(2.71 \pm 1.12) \times 10^8$ [e]	−0.20[c]	1.75×10^8 [c]	0.08−0.15[c]

[a] Reference 10. [b] Reference 11. [c] Reference 12. [d] Reference 13. [e] Reference 20.

values, about 50 at the MP4 level (see Table 6). The κ_2 value calculated at PMP2 level is about two times larger than those obtained at other level of calculations, because of PMP2 $RC_{(I)}$ stabilization is about 2 kcal/mol larger than those predicted by all of the other tested methods. Two features of the barrier of the acidic hydrogen abstraction path are responsible for its very large tunneling factor: (i) its height when the reactant complex is taken into account (it is larger, for the acidic path, by about 6 kcal/mol) and (ii) the larger imaginary frequency of this path (3171.8 cm^{-1} compared to 2319.3 cm^{-1} at the MP2 level), which yields a relatively narrow barrier.

The one-dimensional Eckart potential barriers of paths I and II that have been used to calculate the tunneling factors κ_2 and κ_4 are shown in Figure 3. We used the following Eckart function, $V(x)$:

$$V(s) = \frac{AY}{1+Y} + \frac{BY}{(1+Y)^2} + V_0 \tag{8}$$

where

$$Y = e^{x - x_0/\beta} \tag{9}$$

$$A = V(x = +\infty) - V(x = -\infty) \tag{10}$$

$$B = (2E^* - A) + 2\sqrt{E^*(E^* - A)} \tag{11}$$

$$V_0 = \sum E_{\text{React}} \tag{12}$$

$$x_0 = -\beta \ln\left(\frac{A+B}{B-A}\right) \tag{13}$$

$$\beta = \sqrt{-\frac{2E^*(E^* - A)}{\mu(\nu^*)^2 B}} \tag{14}$$

In the formulas above, E^* is the ZPE corrected barrier height, E_{React} is the ZPE energy of each reactant, ν^* is the imaginary frequency at the transition state, μ is the scaling mass (set equal to 1.0 amu in this work), A and B are independent parameters, x_0 determines the location of the maximum of $V(x)$ along the x axis (it was set at $x = 0$), and β is a range parameter.

Multidimensional semiclassical zero- and small-curvature tunneling methods,[49] denoted as ZCT and SCT, respectively, were also used in order to verify the reliability of the Eckart tunneling calculation. These methods require geometry, energy, gradient, and Hessian information along the minimum energy path (MEP). The ZCT method restricts the tunneling path to the MEP, whereas the SCT method allows the tunneling path to cut corners because of the reaction path curvature. The SCT approach is expected to offer the most accurate treatment of tunneling. Unfortunately, because of the instability of the products wave function discussed above, the IRC calculation does not work properly at the highest levels of calculation, with the number of points being too small to perform a reliable multidimensional tunneling calculation. As a compromise, a 200 point IRC was obtained at the HF/STO-3G level of theory, and new transmission coefficients were calculated for the acidic path at 298.15 K using the kinetic programs available online at the Virtual Lab site.[50] The values $\kappa_{ZCT} = 3.818 \times 10^4$, $\kappa_{SCT} = 8.913$

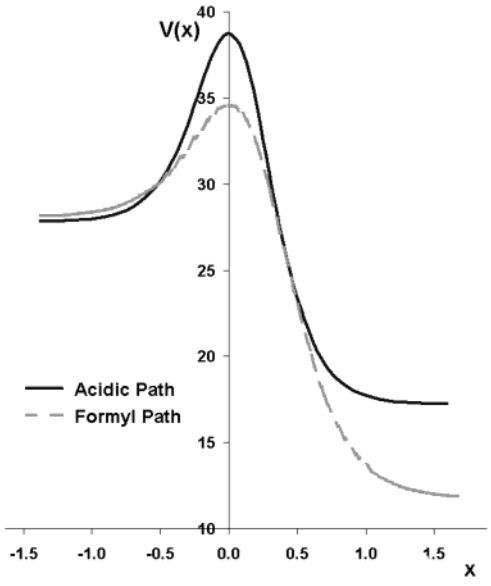

Figure 3. Unidimensional Eckart barriers of the acidic and formyl abstraction, obtained using the PMP4/6-311+G(2d,2p)//MP4/6-311++G-(d,p) energy values and the imaginary frequencies calculated at the MP2/6-311++G(2d,2p) level.

TABLE 7: $\langle S^2 \rangle$ Values before Projection

	S^2			
	$CR_{(I)}$	$CR_{(II)}$	$TS_{(I)}$	$TS_{(II)}$
CCSD(T)/6-311++G(2d,2p)//B3LYP/6-311++G(d,p)	0.758	0.756	0.762	0.765
CCSD(T)/6-311++G(2d,2p)//BH&HLYP/6-311++G(d,p)	0.756	0.756	0.770	0.787
PMP2/6-311++G(2d,2p)//MP2/6-311++G(2d,2p)	0.756	0.756	0.785	0.779
PMP4/6-311++G(2d,2p)//MP4/6-311++G(d,p)	0.757	0.756	0.793	0.783
CCSD(T)/6-311++G(2d,2p)//MP2/6-311++G(2d,2p)	0.757	0.756	0.788	0.779
CCSD(T)/6-311++G(2d,2p)//MP4/6-311++G(d,p)	0.757	0.756	0.793	0.783
CCSD(T)/6-311++G(2d,2p)//QCISD/6-311++G(d,p)	0.757	0.756	0.802	0.782

TABLE 8: Comparison between Kinetic Parameters Obtained at the PMP2/6-311++G(2d,2p)//MP2/6-311++G(2d,2p) Level, Using Calculated and Experimental Heats of Reaction

	κ_2	κ_4	$k_{(I)}$ (L mol^{-1} s^{-1})	$k_{(II)}$ (L mol^{-1} s^{-1})	$k = k_{(I)} + k_{(II)}$ (L mol^{-1} s^{-1})	Ea^{Arr}	A	Γ_{II}
calculated ΔH's	14251.8	52.7	1.98×10^8	1.91×10^7	2.17×10^8	−0.80	5.28×10^7	0.08
experimental ΔH's	15580.1	51.9	2.16×10^8	1.88×10^7	2.35×10^8	−0.91	4.81×10^7	0.08

$\times 10^4$, and $\kappa_{Eckart} = 5.912 \times 10^4$ were obtained. It can be seen that the Eckart tunneling factor lies between those obtained using multidimensional methods. These results are even higher than those reported in Table 6, probably because of the poor level of calculation used to obtain the MEP, but they certainly suggest that the Eckart approach is reliable enough for the HCOOH + OH reaction over the studied temperature range. Similar results on a different reaction that also presents a substantial energy barrier, were previously reported by Truong.[51]

The formyl branching ratio ($\Gamma_{II} = k_{II}/k$) is also reported in Table 6 for all of the methods used in this work. According to the experimental results reported by Singleton et al.,[12] this ratio should be about 0.08−0.15. The PMP4 Γ_{II} suggests that at this level of theory our acidic rate coefficient is slightly underestimated, whereas the PMP2 Γ_{II} shows the best agreement with the experimental results.

The rate coefficients at 298.15 K (Table 6) show a good agreement between the calculated values and the experimental ones, with the exception of the DFT methods. Taking into account the calculated overall rate coefficients as well as the branching ratios the best description of the kinetics of the HCOOH + OH reaction is obtained at the PMP2/6-311++G(2d,2p)//MP2/6-311++G(2d,2p) method. The finding that DFT rate coefficients are too low suggests that in the geometry discrepancy discussed above are the DFT structures which are not correct.

The finding that PMP2 and PMP4 results agree better than the CCSD(T) ones with the experiment may be partially explained by the fact that, in the first case, spin contamination is eliminated by projection. Also, geometries have not been optimized at the CCSD(T) level. The values of $\langle S^2 \rangle$ obtained with all of the methods employed in this work are reported in Table 7. It can be seen that, in the systems studied here, spin contamination is never very large.

There is an important difference between the Arrhenius activation energy, which corresponds to the temperature dependence of the overall rate constant, and the activation energies of each step of the complex mechanism, which only depend on the energies of the stationary points involved. Consequently, they may not have similar values. The mechanism of the HCOOH + OH reaction proposed in this work is complex, and the activation energy of the second step is appreciably positive, which explains why the reaction is not diffusion-controlled.

The temperature dependence of the rate coefficients (k, k_I, and k_{II}) for the HCOOH + OH reaction was also studied (Table 6). The calculated Arrhenius parameters show the best agreement with the experimental values at PMP2/6-311++G(2d,2p)//MP2/6-311++G(2d,2p) and PMP4(SDTQ)/6-311++G(2d,2p)//MP4(SDQ)/6-311++G(d,p) levels of calculation. The Arrhenius plots are shown in Figure 4. The energies and frequencies used were obtained at the PMP2/6-311++G(2d,2p) level of calculation. The two parameter equation for the overall rate coefficient is $k = (5.28 \pm 2.35) \times 10^7 \exp[(404 \pm 125)/T]$ L mol^{-1} s^{-1}. This expression shows a weak temperature dependence, with an activation energy which is slightly negative, and in good agreement with the previously reported ones.[10,12] In addition, the best fit for the acidic and the formyl channels were found to be $k_I = (1.37 \pm 0.40) \times 10^7 \exp[(786 \pm 87)/T]$ and $k_{II} = (5.93 \pm 1.39) \times 10^8 \exp[(-1036 \pm 72)/T]$ L mol^{-1} s^{-1}, respectively. According to these results, the Arrhenius activation energy for the formyl abstraction is 1.09 kcal/mol higher than the one for the acidic abstraction, in perfect agreement with the results in ref 11 an 12.

To evaluate the influence of the errors in the heat of reaction on the kinetic parameters, these were recalculated at the PMP2/6-311++G(2d,2p)//MP2/6-311++G(2d,2p) level, and the experimental heats of reactions were used in the tunneling calculations (Table 8). Our results suggest that the discrepancies in the values of the ΔH's have a very small influence on the kinetic parameters and that the methodology used in this work is reliable.

The fact that the experimental Arrhenius activation energy of the HCOOH + OH reaction is smaller than the one for

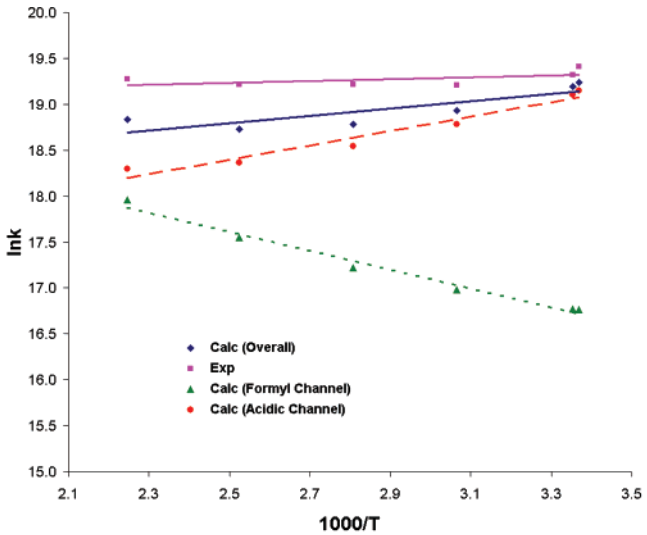

Figure 4. Temperature dependence of k, k_I, and k_{II}, at the PMP2/6-311++G(2d,2p)//MP2/6-311++G(d,P) level.

HCHO + OH can be explained as a consequence of the unusually large tunneling effect of the formic acid reaction. The formaldehyde + OH hydrogen abstraction is also a complex reaction, involving the formation of a reactants complex. In this reaction, the stabilization energy of the complex is about 3 kcal/mol, with the value depending on the method of calculation.[17] The corresponding value for the acidic channel of the OH + formic acid reaction is 4.8 kcal/mol. However, the tunneling factor in the HCHO + OH reaction is only 5.7 at the CCSD-(T)/6-311++G(d,p)//MP2(FC)6-311++G(2d,2p) level, to be compared with $\kappa_2 = 8063.6$ (Table 6).

Additionally, the fact that the rate coefficient of the OH abstraction from formaldehyde is about 1 order of magnitude larger than that from formic acid despite their very similar Arrhenius activation energy can be justified by the larger preexponential factor (*A*) of the former one. The difference in the *A*'s can be explained by the existence of a looser transition structure of the aldehyde,[17] which causes an entropic factor for this reaction larger than the corresponding one for abstraction from formic acid. In addition, both of the apparent activation energies are alike because of the very large tunneling in the formic abstraction, whereas the energy barriers are quite different. Not only does this tunneling decrease dramatically the activation energy but it also reduces the preexponential factor. The conjunction of all of these features may explain the difference between *k*(formaldehyde) and *k*(formic acid).

The calculated activation energies are very different from the Arrhenius experimental ones. Yet, our results offer a plausible explanation for the observed experimental behavior, based on the existence of a very stable prereactive complex, which gives rise to a large and narrow effective barrier, especially in the acidic abstraction. As a consequence, the tunneling correction is remarkably high. That the O−H bond is stronger than the C−H one is in agreement with the higher activation energy obtained for the hydrogen abstraction from the OH group. Nevertheless the acidic path is more likely to occur than the formyl one because the former has both a higher preexponential factor and a much larger tunneling effect. Thus, the acidic rate coefficient is substantially larger than the formyl one.

Conclusions

Two competitive channels for the OH hydrogen abstraction reaction from formic acid have been considered, corresponding to abstraction of either the acidic or the formyl hydrogen atom. In agreement with experimental results, the former is found to contribute more to the overall rate constant. Yet, the existence of the two channels explains the observed non-Arrhenius behavior of the reaction.

Both paths are complex reactions. Each of them consists of a barrierless first step leading to the formation of a prereactive complex, followed by a second step, involving a relatively high activation energy to yield the products. For the acidic channel, the reactant complex is found to be considerably more stable than for the formyl channel. In addition, its transition state barrier is higher, thus giving rise to a larger barrier. This, together with the fact that the barrier along the acidic channel is narrower and that the heat of the reaction for this channel is very small, leads to a huge tunneling effect and to a larger rate constant coefficient than for the formyl abstraction channel. Thus, although the calculated energy barrier of the acidic path is the largest, it is the favored path.

The excellent agreement between the theoretical and experimental overall rate coefficients suggest that the mechanism proposed in this work is adequate to describe the OH + HCOOH reaction. Best results are obtained with the PMP2/6-311++G-(2d,2p)//MP2/6-311++G(2d,2p). Satisfactory results are also obtained with the PMP4 and coupled cluster method.

The temperature dependence of the overall rate constant in L mol^{-1} s^{-1} can be described by the expression $k = (5.28 \pm 2.35) \times 10^7 \exp[(404 \pm 125)/T]$. In the same units, the rate constants for the acidic and formyl channels are $k_I = (1.37 \pm 0.40) \times 10^7 \exp[(786 \pm 87)/T]$ and $k_{II} = (5.93 \pm 1.39) \times 10^8 \exp[(-1036 \pm 72)/T]$, respectively.

Acknowledgment. The authors gratefully acknowledge the financial support from the Instituto Mexicano del Petróleo (IMP) through programs G00058 and FIES-95-97-VI. We also thank the IMP Computing Center for supercomputer time on SGI Origin 2000. The authors also thank Professors W. T. Duncan, R. L. Bell, and T. N. Truong for providing The Rate program through the Internet and Professor R. Atkinson for his valuable suggestions.

References and Notes

(1) Legrand, M.; de Angelis, M. *J. Geophys. Res.* **1995**, *100*, 1445.
(2) Granby, K.; Egeløv, A. H.; Nielsen, T.; Lohse, C. *J. Atmos. Chem.* **1997**, *28*, 195−207.
(3) Johnson, B. J.; Dawson, G. A. *J. Atmos. Chem.* **1993**, *17*, 123.
(4) Glasius, M.; Wessel, S.; Christensen, C. S.; Jacobsen, J. K.; Jørgensen, H. E.; Klitgaard, K. C.; Petersen, L.; Rasmussen, J. K.; Stroyer Hansen, T.; Lohse, C.; Boaretto, E.; Heinemeier, J. *Atmos. Env.* **2000**, *34: 15*, 2471.
(5) Staudt, M.; Wolf, A.; Kesselmeier, J. *Biogeochemistry* **2000**, *48: 2*, 199.
(6) Kesselmeier, J. *J. Atmos. Chem.* **2001**, *39:3*, 219.
(7) Altshuller, A. P. *J. Atmos. Chem.* **1991**, *13*, 131.
(8) Atkinson, R. *Atmos. Environ.* **1990**, *24A*, 1.
(9) Glasius, M.; Wessel, S.; Christensen, C. S.; Jacobsen, J. K.; Jorgensen, H. E.; Klitgaard, K. C.; Petersen, L.; Rasmussen, J. K.; Hansen, T. S.; Lohse, C.; Boaretto, E.; Heinemeier, J. *Atmos. Env.* **2000**, *34*, 2471.
(10) Wine, P. H.; Astalos, R. J.; Mauldin, R. L., III. *J. Phys. Chem.* **1985**, *89*, 2620.
(11) Jolly, G. S.; McKenney, D. J.; Singleton, D. L.; Paraskevopoulos, G.; Bossard, A. R. *J. Phys. Chem.* **1986**, *90*, 6557.
(12) Singleton, D. L.; Paraskevopoulos, G.; Irwin, R. S.; Jolly, G. S.; McKenney, D. J. *J. Am. Chem. Soc.* **1988**, *110*, 7786.
(13) Dagaut, P. *Int. J. Chem. Kinet.* **1988**, *20*, 331.
(14) Zetzsch, C.; Stuhl, F. In *Physicochemical Behaviour of Atmospheric Pollutants*, version B; Ott, H., Ed.; Proceedings of the Second European Symposium; Reidel: Dordrecht, 1982; p 129.
(15) Alvarez-Idaboy, J. R.; Mora-Diez, N.; Vivier-Bunge, A. *J. Am. Chem. Soc.* **2000**, *122*, 3715.
(16) Uc, V. H.; García-Cruz, I.; Hernández-Laguna, A.; Vivier-Bunge, A. *J. Phys. Chem. A* **2000**, *104*, 7847.
(17) Alvarez-Idaboy, J. R.; Mora-Diez, N, Boyd, R. J.; N.; Vivier-Bunge, A. *J. Am. Chem. Soc.* **2001**, *123*, 2018.
(18) Galano, A.; Alvarez-Idaboy, J. R.; Montero-Cabrera, L. A.; Vivier-Bunge, *J. Comput. Chem.* In press.
(19) DeMore, W. B.; Sander, S. P.; Golden, D. M.; Hampson, R. F.; Kurylo, M. J.; Howard, C. J.; Ravishankara, A. R.; Kolb, C. E.; Molina, M. J. *JPL Publ.* **1997**, *97*, 4.
(20) Atkinson, R.; Baulch, D. L.; Cox, R. A.; Hampson, R. F., Jr.; Kerr, J. A.; Rossi, M. J.; Troe, J. *J. Phys. Chem. Ref. Data* **1999**, *28* (2), 191.
(21) Frisch, M. J.; Trucks, G. W.; Schlegel, H. B.; Scuseria, G. E.; Robb, M. A.; Cheeseman, J. R.; Zakrzewski, V. G.; Montgomery, J. A., Jr.; Stratmann, R. E.; Burant, J. C.; Dapprich, S.; Millam, J. M.; Daniels, A. D.; Kudin, K. N.; Strain, M. C.; Farkas, O.; Tomasi, J.; Barone, V.; Cossi, M.; Cammi, R.; Mennucci, B.; Pomelli, C.; Adamo, C.; Clifford, S.; Ochterski, J.; Petersson, G. A.; Ayala, P. Y.; Cui, Q.; Morokuma, K.; Malick, D. K.; Rabuck, A. D.; Raghavachari, K.; Foresman, J. B.; Cioslowski, J.; Ortiz, J. V.; Stefanov, B. B.; Liu, G.; Liashenko, A.; Piskorz, P.; Komaromi, I.; Gomperts, R.; Martin, R. L.; Fox, D. J.; Keith, T.; Al-Laham, M. A.; Peng, C. Y.; Nanayakkara, A.; Gonzalez, C.; Challacombe, M.; Gill, P. M. W.; Johnson, B. G.; Chen, W.; Wong, M. W.; Andres, J. L.; Head-Gordon, M.; Replogle, E. S.; Pople, J. A. *Gaussian 98*, revision A.3; Gaussian, Inc.: Pittsburgh, PA, 1998.
(22) Curtiss, L. A.; Raghavachari, K.; Redfern, P. C.; Rassolov, V.; Pople, J. A. *J. Chem. Phys.* **1998**, *109*, 7764.
(23) Duncan, W. T.; Bell, R. L.; Truong, T. N. *J. Comput. Chem.* **1998**, *19*, 1039.

(24) Robinson, P. J.; Holbrook, K. A. *Unimolecular Reactions*; Wiley−Interscience: London, 1972.
(25) Rayez, M. T.; Rayez, J. C.; Sawerysyn, J. P. *J. Phys. Chem*. **1994**, *98*, 11342.
(26) Talhaoui, A.; Louis, F.; Devolder, P.; Meriaux, B. Sawerysyn, J. P.; Rayez, M. T.; Rayez, J. C. *J. Phys. Chem.* **1996**, *100:32*, 13531.
(27) Benson, S. W. *Thermochemical Kinetics*, 2nd ed.; Wiley: New York, 1976.
(28) http://www.iupac-kinetic.ch.cam.ac.uk/.
(29) Atkinson, R. Private communication.
(30) Peyerimhoff, S. D.; Skell, P. S.; May, D. D.; Buenker, R. J. *J. Am. Chem. Soc.* **1982**, *104*, 4515.
(31) Feller, D.; Huyser, E. S.; Borden, W. T.; Davidson, E. R. *J. Am. Chem. Soc.* **1983**, *105*, 1459.
(32) Malean, A. D.; Lengsfield, B. H.; Pacansky, J.; Ellinger, Y. *J. Chem. Phys.* **1985**, *83*, 3567.
(33) Burton, N.; Yamaguchi, Y.; Alberts, I. L.; Schaefer, H. F. *J. Chem. Phys.* **1991**, *95*, 7466.
(34) Kudla, K.; Schatz, G. C. *J. Phys. Chem.* **1991**, *95*, 8267.
(35) Francisco, J. S. *J. Phys. Chem.* **1991**, *95*, 1167.
(36) Stanton, J. F.; Gauss, J. *J. Chem. Phys.* **1994**, *101*, 8938.
(37) Rauk, A.; Yu, D.; Borowski, P.; Roos, B. *Chem. Phys.* **1995**, *197*, 73.
(38) Stanton, J. F.; Kadagathur, N. S. *J. Mol. Struct.* **1996**, *376*, 469.
(39) Ayala, P. Y.; Schlegel, H. B. *J. Chem. Phys.* **1998**, *108*, 7560.
(40) Crawford, T. D.; Stanton, J. F. *J. Chem. Phys.* **2000**, *112*, 7873.
(41) Formosinho, S. J.; Csizmadia, Y. G.; Arnaut, L. G. *Theoretical and Computational Models for Organic Chemistry*; Kluwer: Dordrecht, 1991; p 159.
(42) Arteca, G. A.; Mezey, P. G. *Int. J. Quantum Chem., Quantum Chem. Symp.* **1990**, *24*, 1.
(43) Arteca, G. A.; Mezey, P. G. *J. Phys. Chem.* **1989**, *9*, 4746.
(44) Arteca, G. A.; Mezey, P. G. *Int. J. Quant. Chem., Quantum Chem. Symp.* **1990**, *24*, 1.
(45) Salem, L. *Electrons in Chemical Reactions*; Wiley: New York, 1982; Chapter 2.
(46) Kim, S. S.; Kim, H. R.; Kim, H. B.; Youn, S. J.; Kim, C. J. *J. Am. Chem. Soc.* **1994**, *116*, 2754.
(47) Colthurst, M. J.; Williams, A. *J. Chem. Soc., Perkin Trans.* **1997**, *2*, 1493.
(48) Donahue, N. M. *J. Phys. Chem. A* **2001**, *105*, 1489.
(49) Truhlar, D. G.; Isaacson, A. D.; Skodje, R. T.; Garret, B. C. *J. Phys. Chem.* **1982**, *86*, 2252.
(50) http://vklab.hec.utah.edu/.
(51) Truong, T. N. *J. Phys. Chem. B* **1997**, *101*, 2750.